nature communications

Article

https://doi.org/10.1038/s41467-025-55937-4

All-angle unidirectional flat-band acoustic metasurfaces

Received: 2 May 2024

Accepted: 2 January 2025

Published online: 14 January 2025

Check for updates

Chenglin Han[1,2,3,4,10], Shida Fan[1,10], Hong-Tao Zhou[3,5,10], Kuan He[1], Yurou Jia[3,6], Changyou Li[1], Hongzhu Li[5], Xiao-Dong Yang[7,8] ✉, Li-Qun Chen[9], Tianzhi Yang[1,2,4] ✉ & Cheng-Wei Qiu[3] ✉

Flat bands have empowered novel phenomena such as robust canalization with strong localization, high-collimation and low-loss propagation. However, the spatial symmetry protection in photonic or acoustic lattices naturally forces flat bands to manifest in pairs aligned at an inherently specific angle, resulting in a fixed bidirectional canalization. Here, we report an acoustic flat-band metasurface, allowing not only unidirectional canalization at all in-plane angles but also robust tunability in band alignment. The twist, tilt, and skew angles of the bilayer metasurface can be flexibly controlled to break both in-plane and out-of-plane spatial symmetries. These features can thereby turn arbitrary twist angles between bilayers into 'magic angles', while maintaining all unidirectional canalization and band alignment tunability. This work may significantly contribute to pushing twisted moiré physics into higher dimensions and facilitate the application of advanced acoustic or optical devices.

The magic angle, a unique phenomenon observed in twisted moiré systems, has captured considerable attention across various fields spanning from electronics and photonics to phononics[1–12]. It represents a critical point where the interlayer interactions reach a delicate balance, giving rise to the emergence of unconventional flat bands[13,14]. Benefitting from the minimal dispersion features, bilayer moiré lattices at the magic angle allow for the rapid transport of electrons, photons, and phonons in a quasi-lossless manner[15–19]. This groundbreaking discovery opens up new opportunities for customizing sensing devices with exceptional electrical, optical, and acoustic properties[20–23].

Recently, a distinct class of flat bands with topological transition has emerged within highly anisotropic twisted moiré systems[24–27]. Leveraging a tailored hyperbolic dispersion relationship, wave propagation within each layer is predominantly confined to a single principal direction in the plane, while undergoing rapid attenuation in the perpendicular orientation[28]. Furthermore, the pronounced interlayer interactions intricately hybridize the dispersion relationships upon the superposition of two such twisted layers[29,30]. With variations in the twist angle, the dispersion curve transitions from an open hyperbolic to a closed elliptical shape. At the magic angle, a critical state is reached, showcasing exceptional flatness. During this phase, wave propagation exhibits strong localization, high collimation, and low loss[31,32]. These unique features further distinguish the twisted system as the only known entity with such superior wave characteristics[33,34].

However, several significant inherent limitations persist within twisted bilayer moiré systems despite some advancements. The limited magic angles constrain the canalization direction of the flat band to be fixed in several directions at each operating frequency[35,36]. Furthermore, the magic-angle-induced flat band has exclusively maintained mirror-symmetrical bidirectional polarization. These

[1]School of Mechanical Engineering and Automation, Northeastern University, Shenyang, China. [2]Key Laboratory of Vibration and Control of Aero-Propulsion System, Ministry of Education, Northeastern University, Shenyang, China. [3]Department of Electrical and Computer Engineering, National University of Singapore, Singapore, Singapore. [4]Electrobiomaterials Institute, Key Laboratory for Anisotropy and Texture of Materials (Ministry of Education), Northeastern University, Shenyang, China. [5]Department of Mechanics, School of Mechanical Engineering, Tianjin University, Tianjin, China. [6]Department of Physics, MOE Key Laboratory of Modern Acoustics, Collaborative Innovation Center of Advanced Microstructures, Nanjing University, Nanjing, China. [7]School of Aerospace Engineering, Shenyang Aerospace University, Shenyang, China. [8]Department of Mechanics, Beijing University of Technology, Beijing, China. [9]School of Science, Harbin Institute of Technology, Shenzhen, China. [10]These authors contributed equally: Chenglin Han, Shida Fan, Hong-Tao Zhou.
✉e-mail: jxdyang@163.com; yangtianzhi@me.neu.edu.cn; chengwei.qiu@nus.edu.sg

imperfections significantly limit the flexibility and diversity of bilayer moiré systems in practical applications.

Here, we propose the concept of a symmetry-broken moiré system to directly eliminate these inherent constraints in the existing bilayer configuration. All twisted angles can be turned to be "magic angles" by breaking the in-plane symmetry in each lattice of our bilayer metamaterial. More importantly, by further breaking the out-of-plane symmetry, tunable unidirectional canalization with flat band alignment can be achieved, marking another significant distinction from all previous magic-angle-related reports featuring bidirectional canalization[13,22]. As a proof of concept, we theoretically and experimentally demonstrate a bilayer acoustic moiré system incorporating nonlocal hyperbolic metasurfaces. The spatial symmetry of the bilayer moiré system is tailored by adjusting the introduced tilt and skew angles along both in-plane and out-of-plane directions. The broken symmetry eliminates the sole dependence on the twist angle and creates a more intricate interlayer coupling mechanism, thus enabling the tunability of canalization direction and orientation.

Results

Symmetry-broken bilayer moiré metasurfaces

Figure 1a shows the schematic of the proposed symmetry-broken bilayer moiré metasurfaces. It consists of two tight stacks of nonlocal hyperbolic acoustic metasurfaces with in-plane deformation and out-of-plane tilt. The periodic supercell in each monolayer resembles a triclinic configuration, defined by the skew angle (β) in the x-y plane, and the tilt angle (γ) in the y-z plane. The evolution of symmetry breaking is illustrated in Fig. 1b. In-plane and out-of-plane symmetries are broken by introducing non-zero values for β and γ, respectively. The further control of the twist angle (θ) between the two layers will allow the symmetry-broken moiré system to achieve the unidirectional canalization in any direction (φ).

To implement the concept, each monolayer nonlocal metasurface is designed to maintain the hyperbolic state through the inductive ($\mathrm{Im}[Z_x] < 0$) and capacitive ($\mathrm{Im}[Z_y] > 0$) impedance along the x- and y-axis directions, respectively. A relatively broad bandwidth, ranging from 2400 to 2750 Hz, ensures robust hyperbolic properties (see Supplementary Fig. S1a). For the bilayer moiré system without symmetry breaking, the twisting operation can produce two distinct modes: hyperbolic and elliptical, under the modulation of the interlayer coupling. In particular, a unique flat band emerges as a new hybridized state at the magic angle, facilitating low-loss propagation with canalization mode (Fig. 1c). At non-magic twist angles, the hybrid states exhibiting either hyperbolic or elliptical hinder the possibility of forming canalization. However, this topological transition from hyperbolic to elliptical mode is determined by the anticrossing point (N_{ACP})[36–39]. Due to the magic angle ($\theta \approx 23°$) within $0° \sim 90°$, the flat band appears only once, resulting in its fixed orientation. It is noted that three additional magic angles are also obtained due to the mirror symmetry.

In contrast, the direction of canalization can be flexibly controlled in the bilayer moiré system with low symmetry similar to triclinic crystals[40,41]. Specifically, when the in-plane symmetry is broken (middle of Fig. 1b), it is found that the canalization can sweep over all directions in the plane (Fig. 1d). This is mainly attributed to that the introduced β tunes the orientation of hyperbolic dispersion and further affects the hybridized modes. In bilayer, anisotropic moiré systems twisted to the magic angle, the hyperbolic dispersion curves of the upper and lower layers hybridize due to interlayer coupling, forming flat bands that enable canalization[36]. However, since the shapes of the hyperbolic dispersion curves are fixed, the curves of the upper and lower layers can only hybridize to form canalization at a relatively specific angle (the magic angle). The introduction of the skew angle disrupts the in-plane symmetry, geometrically twisting the hyperbolic dispersion of each layer (as shown in Supplementary Fig. S1). This change, through the hybridization of interlayer coupling, further modifies the overall dispersion of the bilayer system. Thus, this allows the hybridized flat bands to adjust the canalization direction without changing the magic angle. Furthermore, similar to ghost mode[42,43], when the out-of-plane symmetry is broken (right side of Fig. 1b), the introduced γ disrupts the

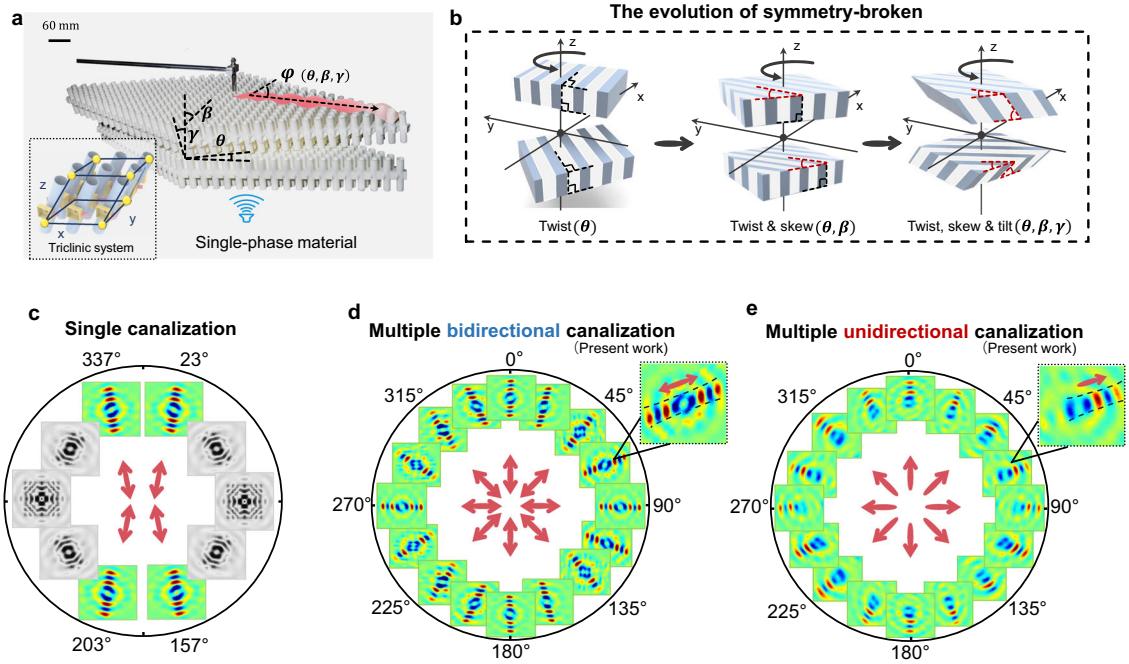

Fig. 1 | Symmetry-broken bilayer moiré system with multiple unidirectional canalization. a Schematic of the symmetry-broken bilayer moiré system with unidirectional sound propagation. The inset shows an enlarged diagram of the supercell. **b** Evolution process regarding the in-plane and out-of-plane symmetry breaking. **c**–**e** Patterns of canalization at the magic-angle-induced flat band for the bilayer moiré system with varying levels of symmetry breaking: none, in-plane, or both in-plane and out-of-plane.

https://doi.org/10.1038/s41467-025-55937-4

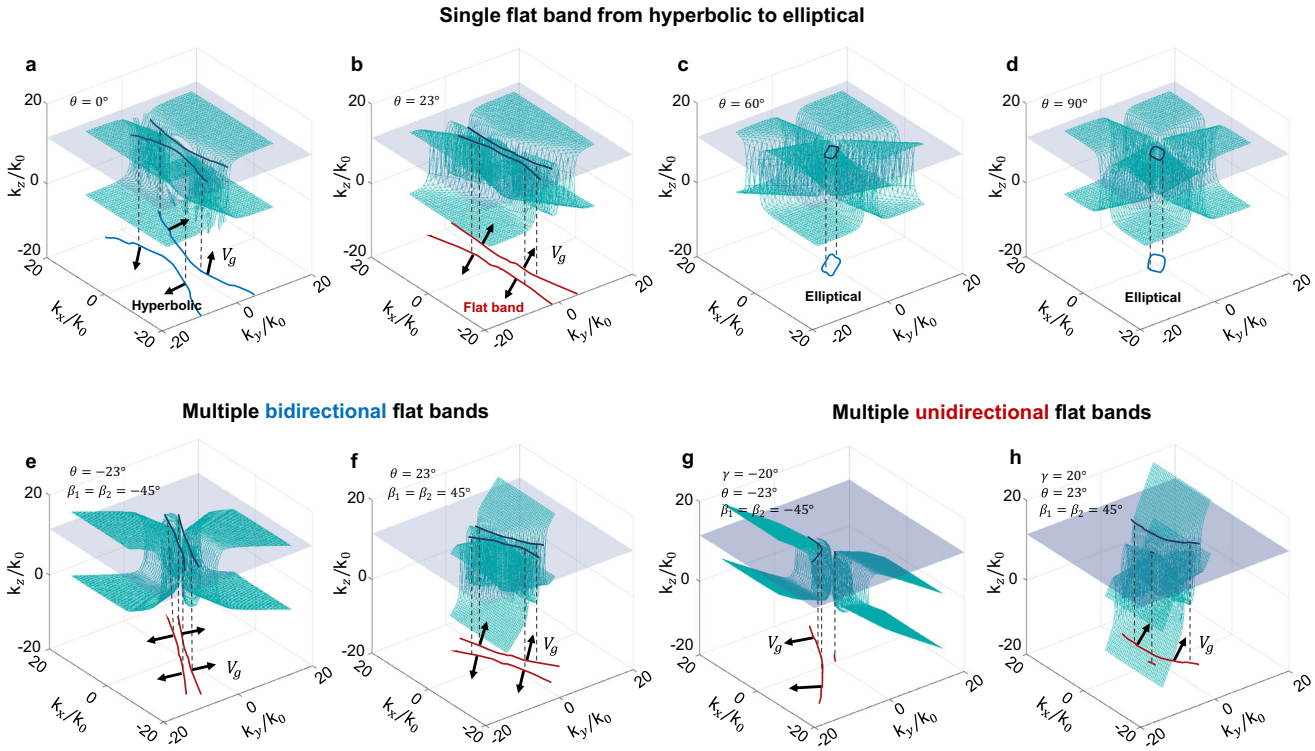

Fig. 2 | Theoretical prediction on hybridized dispersion curves. **a**–**d** Conventional topological transition from hyperbolic to elliptic. **e**, **f** Multiple bidirectional flat bands generated by breaking in-plane symmetry, where θ is unchanged and β_1 and β_2 is changed to tune the direction of the flat bands. **g**, **h** Multiple unidirectional flat bands generated by breaking both in-plane and out-of-plane symmetries. There is only one curve in the flat band after adding γ. The top of each subpanel shows the dispersion shape predicted by the theory model, while the bottom shows the predicted curve on the upper surface of the system.

central symmetry of the original dispersion curve. Strong unidirectional propagation is observed in the *x*-*y* plane. In addition, unidirectional canalization in all directions can also be achieved by combining with β adjustments (Fig. 1e). This suggests that it is feasible to implement multiple unidirectional flat bands in the bilayer moiré system. Detailed geometrical parameters of unit cells are presented in Supplementary S2.

Theoretical model on multiple unidirectional flat bands

To elucidate the formation mechanism of multiple flat bands, we establish a theoretical model for solving the hybridized dispersion curves in the symmetry-broken moiré system. Based on the Bloch-Floquet theorem and Transfer Matrix method[44], the dispersion relationship of monolayer metasurface can be initially solved (see Supplementary S3). The introduced θ, β and γ for each monolayer will modulate the in-plane wavevectors as follows:

$$\begin{pmatrix} \mathbf{k_{x1}} \\ \mathbf{k_{y'}} \end{pmatrix} = \begin{pmatrix} \cos(\theta) & -\sin(\theta) \\ \sin(\theta) & \cos(\theta) \end{pmatrix} \begin{pmatrix} \mathbf{k_x} \\ \mathbf{k_y} \end{pmatrix} \quad (1)$$

$$\mathbf{k_{y1}} = \mathbf{k_{y'}}\cos(\beta) + \mathbf{k_{x1}}\sin(\beta) \quad (2)$$

$$\mathbf{k_{z1}} = \mathbf{k_z}\cos(\gamma) + \mathbf{k_{y'}}\sin(\gamma) \quad (3)$$

where $\mathbf{k_z^2} = \mathbf{k_0^2} - \mathbf{k_x^2} - \mathbf{k_y^2}$ with $\mathbf{k_x}$, $\mathbf{k_y}$ and $\mathbf{k_z}$ being the original wavevector components in the *x*-, *y*- and *z*-directions, respectively; $\mathbf{k_{x1}}$, $\mathbf{k_{y1}}$ and $\mathbf{k_{z1}}$ are the corresponding modulated wavevector components after introducing θ, β, and γ. By solving Eqs. (1)–(3), the final dispersion relationship of $\mathbf{k_{x1}}$, $\mathbf{k_{y1}}$ and $\mathbf{k_{z1}}$ can be obtained. Note that θ, β, and γ are oriented to be positive in the counterclockwise direction. In addition, it can be clearly observed that $\mathbf{k_{y1}}$ and $\mathbf{k_{z1}}$ are tilted about the k_z-axis and the k_{x1}-axis, respectively. Therefore, the broken symmetry effectively eliminates the sole dependence on θ and creates a more intricate interlayer coupling mechanism. Furthermore, based on the transfer matrix, the coupled dispersion relationship for the symmetry-broken bilayer moiré system can be established. At the same time, it can be extended to the multilayered system[39] (see Supplementary S3).

To contrast the difference with and without symmetry breaking, Fig. 2a–d initially presents the theoretically predicted hybridized dispersion curves for the bilayer moiré system without system breaking at different twist angles. It can be observed that the dispersion curve remains hyperbolic at $\theta = 0°$ (Fig. 2a) and gradually becomes flatness with θ approaching 23° (Fig. 2b). For twist angles above 23°, the dispersion gap gradually close and the propagation shifts from open canalization to the closed state (Fig. 2c, d). Conventional topological transition from hyperbolic to elliptic is observed in the theoretical results. However, limited by the N_{ACP} and the fixed opening angle α of the monolayer hyperbolic curve[36], the flat band is only generated in the transition phase of the two modes at $f = 2650$ Hz with $\theta \approx 23°$ (Fig. 2b). The group velocity (V_g) appears in opposite directions, and the singularity of the magic angle can only generate a single acoustic flat band in a fixed direction at this frequency. This severely limits the application potential of the system.

When the in-plane symmetry is disrupted, the introduced β overcomes the limitation, as depicted in Fig. 2e, f. By maintaining $\Delta\theta$ unchanged while tuning β to 45° or −45°, the two groups of flat bands rotate in the plane, and the V_g is significantly deflected compared to Fig. 2b. This occurs because, at a constant twist angle, β controls the deflection of the flat band by simultaneously distorting the dispersion curves of both monolayers, thus producing canalization with diverse orientations (φ). Furthermore, the out-of-plane symmetry breaking reveals that half of the in-plane flat band vanishes, while the other half exhibits highly concentrated group velocity in the same θ (Fig. 2g, h). This leads to the realization of unidirectional low-loss propagation. Similar to bulk anisotropic

https://doi.org/10.1038/s41467-025-55937-4

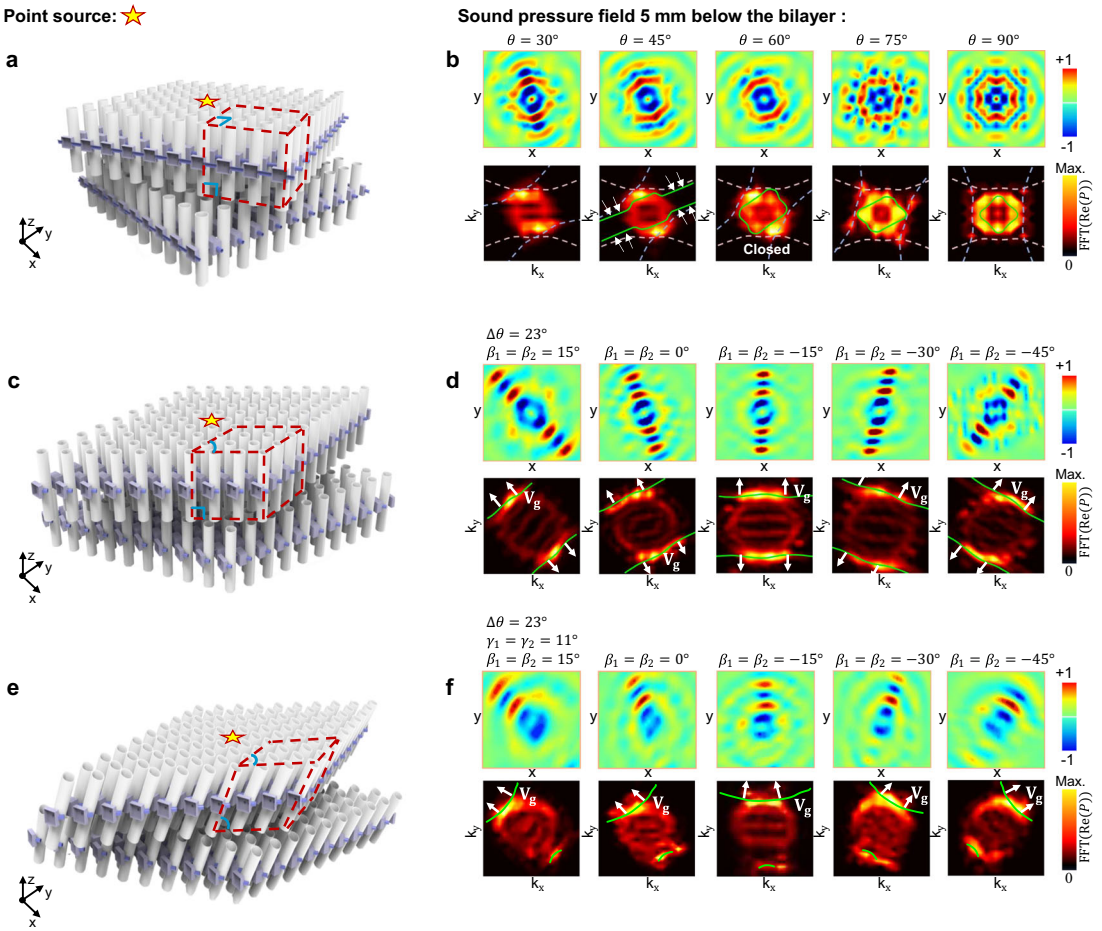

Fig. 3 | Unidirectional and tunable canalization. a, **c**, **e** The schematics on the bilayer moiré system with three levels of symmetry breaking: none, in-plane, or both in-plane and out-of-plane. **b** Pressure field and Fourier spectra at different θ. **d** Pressure field and Fourier spectra at different β. **f** Pressure field and Fourier spectra at the same γ and different β. The green curves are the dispersion curves calculated using the theoretical bilayer model. The dashed curves indicate the dispersion curves of the upper and lower metasurfaces. The simulations are frequency domain simulations. The simulated domains in (**b**, **d**, **f**) are the air surrounding the metasurface, with the metasurface structure modeled as a hard boundary.

crystals[42], the introduction of γ alters the hybridization mode to a "ghost mode" between surface and volume modes. Some energy propagates out of the surface, decaying and disappearing, while others continue to propagate along the surface. This pattern partially pushes the flat band out of the surface and partly keeps it within. This clearly elucidates the construction of multiple unidirectional flat bands with in-plane canalization in any desired direction.

Verification on unidirectional and tunable canalization

To validate the effectiveness of theoretical models, numerical simulations are conducted for the symmetry-broken bilayer moiré system. Figure 3a, c, e illustrates the schematics of the three kinds of symmetry breaking: none, in-plane, or both in-plane and out-of-plane, respectively. The red dashed boxes in Fig. 3a, c, e illustrate the transition of the three metasurface systems from a square pattern to a monoclinic pattern, and finally to a triclinic pattern. The simulated sound fields on the x-y plane at $f = 2650$ Hz and the corresponding Fourier spectra are presented in Fig. 3b, d, f, respectively. It can be seen that sound waves are directed predominantly in one direction at $\theta = 30°$, near the magic angle of 23°. The corresponding Fourier spectrum remains relatively flat. As the twist angle increases, sound waves start to diffuse. The dispersion curve almost closes at $\theta = 60°$, and completely closes at 75° and 90°, resulting in the sound energy spreading in all directions. Therefore, it is challenging to achieve canalization propagation with arbitrary canalization in the absence of symmetry breaking.

However, when we introduce β_1 and β_2 to break the in-plane symmetry, the canalization propagation direction is deflected to different angles, as depicted in Fig. 3d. The dispersion curves are also extremely flat and agree well with the theoretical predictions. Instead of using an intelligent multilayer system[16], we achieve tunable canalization in bilayers. It is noted that omnidirectional tunable canalization can also be achieved due to the 90° symmetry of each monolayer metasurface. Furthermore, by adjusting γ_1 and γ_2 (Fig. 3f), some canalization propagates out-of-plane, enabling the unidirectional canalization. Through simultaneous control of β and γ, unidirectional propagation with tunable canalization is further achieved, showing good consistency with theoretical results.

In addition, we explore the scenario where only one β_1 is controlled without changing γ. Remarkably, the initially diffuse sound field in the moiré system without symmetry breaking is restored to a state of highly concentrated propagation at non-magic twist angles (see Supplementary S4). With a sensible combination of twist and skew angles, all magic angles can theoretically be implemented at will. It is noted that the thermal viscosity loss effects are also considered by adding viscous boundary layers to the numerical simulation[38,45,46]. The negligible influence further highlights the potential for manipulating acoustic waves using symmetry-broken bilayer moiré acoustic metasurfaces.

https://doi.org/10.1038/s41467-025-55937-4

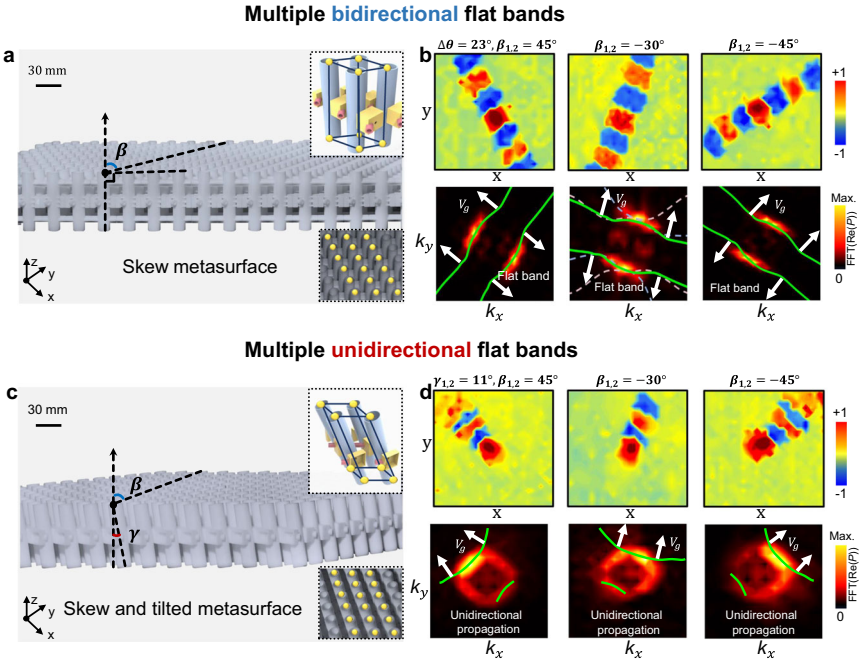

Fig. 4 | Experiment demonstrations of symmetry-broken bilayer moiré system. **a** Photograph of the fabricated sample with in-plane symmetry breaking. The inset shows the enlarged views of the low-symmetry supercell. **b** Measured pressure fields and Fourier spectra with multiple canalization. **c** Photograph of fabricated sample with both in-plane and out-of-plane symmetries breaking. The inset shows the enlarged views of the low-symmetry supercell. **d** Measured pressure fields and Fourier spectra with multiple unidirectional canalization. The green curves present the dispersion curves calculated by the theoretical model.

Experimental demonstrations of unidirectional and tunable canalization

To experimentally validate our concept, three types of bilayer moiré metasurfaces are fabricated using 3D printing (Fig. 1a). The samples are wrapped in acoustic foam to prevent reflections during experiments. Sound waves are emitted from a speaker placed beneath the bilayer moiré system, while two microphones are used to record sound pressures. One is positioned ~30 cm below the sound source, and the other is placed 5 mm above the metasurface. By adjusting β and γ, the in-plane and out-of-plane symmetries can be broken for the fabricated moiré systems, as depicted in Fig. 4a, c. Note that the metasurfaces are only composed of a single-phased solid material, where the microstructural design of each monolayer ensures the anisotropic dispersion relationship. Then the transmitted pressure fields are normalized by the incident sound pressure. The Fourier spectra are further derived from the collected pressure data.

We initially conducted the experimental measurements for the bilayer moiré system without symmetry breaking. Low-loss sound propagation and the flat band in the Fourier spectrum are observed at the theoretical magic angle $\theta \approx 23°$. Topological transition from hyperbolic to elliptic mode is also achieved by changing θ (see Supplementary Fig. S5). Furthermore, the experimental results for the bilayer moiré system with in-plane symmetry breaking are presented in Fig. 4b. It can be clearly observed that the direction of highly concentrated canalization after hybridization is precisely controlled through the introduced β_1 and β_2. In particular, the propagation shifts significantly left for $\beta_1 = \beta_2 = 45°$ and shifts right for $\beta_1 = \beta_2 = -45°$ compared to $\beta_1 = \beta_2 = 0°$. We also fit the Fourier spectra of the three propagation directions to the dispersion curve, showing a perfect match. This alignment with the deflection of the flat band as β changes further validates the effectiveness of the theoretical model.

Figure 4d presents the measured results for the bilayer moiré system with both in-plane and out-of-plane symmetry breaking. When the twist angle is maintained unchanged and introduced $\gamma_1 = \gamma_2 = 11°$, the unidirectional propagation of the sound is successfully achieved. Furthermore, in combination with the directional control of β_1 and β_2, the directional tuning of unidirectional canalization is realized. The obtained Fourier spectra also agree well with the theoretical predictions. In addition, the pressure amplitudes at both ends of each unidirectional propagation path are measured to calculate the transmission ratio. An average unidirectionality ratio of 4.2 is obtained, demonstrating excellent unidirectional propagation properties (see Supplementary S6). It is noted that the symmetry-broken moiré systems can be extended to manipulate various types of sound propagation. In addition, the opening angle can be reduced by increasing the number of stacked layers[23,39]. This is beneficial for broadening the operating bandwidth of unidirectional canalization, thus offering a versatile platform for extreme manipulation of energy flow.

Discussion

In summary, we theoretically and experimentally demonstrate the concept of a symmetry-broken moiré system to directly overcome the limitations of fixed flat bands in bilayer configurations. For multiple canalization, we break the in-plane symmetry to influence N_{ACP}, and further break the out-of-plane symmetry to achieve unidirectional canalization. Thus, the expected unidirectional low-loss propagation with tunable canalization can be achieved without increasing the number of layers. Compared to increasing the number of layers, this method enables more precise tuning of canalization, which is crucial for applications in acoustic or optical devices that require high-precision control. Additionally, such unidirectional systems have c-ritical applications in acoustic isolation, noise control, ultrasound imaging, and non-destructive testing, while unidirectional optical systems show immense potential in optical isolation, high-density data storage, and sensing and detection. Our theoretical model accurately predicts unidirectional flat bands and explains experimental observations. All magic angles can be implemented at will by using a sensible combination of twist and skew angles. It should be noted that this work relies on anisotropy-guided hyperbolic dispersion as the fundamental principle to achieve its objectives[23,37,38,42,44]. However, using periodic

structural modulation and tuning the interlayer coupling distance to achieve in-plane wave confinement is also an effective method[32,47]. Combining the two could lead to interesting results. Additionally, it is worth mentioning that significant progress has been made in asymmetric radiation, unidirectional radiation, and resonance by breaking symmetry[48,49]. Their unidirectional resonance mainly focuses on the far-field radiation characteristics, where the propagation direction and polarization state of light in the far field can be controlled solely by twisting the bilayer metamaterials. In contrast, our research focuses on achieving unidirectional canalized propagation of sound waves within the plane. Not only did we break symmetry, but we also achieved efficient unidirectional canalized propagation in all directions within the plane. This design demonstrates unique advantages in acoustic devices, wave manipulation, and practical applications, significantly expanding the practicality and flexibility of bilayer systems. In the field of light waves or elastic waves, we recommend using columnar nanostructures. By tilting and skewing each columnar structure, it may be possible to tune wave propagation to achieve similar phenomena. The presented work opens new avenues for twisted moiré systems and offers insights for future research in unidirectional flat bands in other fields.

Methods

Numerical simulations

The pressure acoustics module of the COMSOL Multiphysics module was used to perform the numerical simulations. Specifically, the frequency domain and eigenfrequency modules were used. Both sides of the unit cell were configured with Bloch boundary conditions, while the top and bottom surfaces were set as perfectly matched layers (PMLs). The band structure of the crystal cell was then numerically calculated by the eigenfrequency module using a frequency sweep, as shown in Supplementary Figs. S1 and S2. Six PMLs were positioned around the bilayer moiré system to reduce reflections. The point sound source was set above the center of the upper layer. Using the frequency domain module, the pressure field was recorded 5 mm below the metasurface bilayer (see Fig. 3). According to the theoretical dispersion model, the prediction results of the three systems are plotted using MATLAB (Fig. 2).

Sample preparations and measurements

The bilayer moiré system was fabricated using 3D printing, with each metasurface comprising 18 × 18 unit cells. A speaker (13A05-8Ω), with a radius of ~6.0 mm, was positioned at the center of the bilayer system. It is considered a point source and excites omnidirectionally. An acoustic microphone was mounted above the system on a thin mechanical rod driven by a motor to capture the transmitted sound pressure, allowing data collection at various step densities. Grid points were collected at a step size of 8 mm to obtain the plane data. Another reference acoustic microphone was placed ~30 cm below the point sound source to record the incident sound pressure. To unify the sound pressure information measured at different times of the whole sound field, the reference microphone measures the input signal of the speaker at the same time. Acoustic foam was used around and under the system to minimize reflections. The equipment used in our experiment includes a computer, chassis (NI PXIe-1082), power amplifier (E2021), signal generator (DG1022U), motor (9030), two microphones (AWA 14604), a custom-built three-axis motion platform, and a microphone support rod (see Supplementary S7). The corresponding results are depicted in Fig. 4b, d.

Data availability

All relevant data are available in the main text and Supporting Information, and can be obtained from the authors upon request. Source data are provided with this paper.

References

1. Cao, Y. et al. Strange metal in magic-angle graphene with near Planckian dissipation. *Phys. Rev. Lett.* **124**, 076801 (2020).
2. Cao, Y. et al. Unconventional superconductivity in magic-angle graphene superlattices. *Nature* **556**, 43–50 (2018).
3. Jiang, S., Shan, J. & Mak, K. F. Electric field switching of two-dimensional van der Waals magnets. *Nat. Mater.* **17**, 406 (2018).
4. Huang, Y. et al. Pressure controlled magnetism in 2D molecular layers. *Nat. Commun.* **14**, 3186 (2023).
5. Zhang, L. et al. Van der Waals heterostructure polaritons with moiré induced nonlinearity. *Nature* **591**, 61 (2021).
6. Sunku, S. S. et al. Photonic crystals for nanolight in moiré graphene superlattices. *Science* **362**, 1153 (2018).
7. Deng, Y. et al. Magic-angle bilayer phononic graphene. *Phys. Rev. B* **102**, 180304 (2020).
8. Grover, S., Bocarsly, M., Efetov, D. & Zeldov, E. Chern mosaic and Berry-curvature magnetism in magic-angle graphene. *Nat. Phys.* **18**, 885 (2022).
9. Jaoui, A., Levitov, L. & Efetov, D. Quantum critical behaviour in magic-angle twisted bilayer graphene. *Nat. Phys.* **18**, 633 (2022).
10. Yu, J., Kivelson, S. & Feldman, B. Correlated Hofstadter spectrum and flavour phase diagram in magic-angle twisted bilayer graphene. *Nat. Phys.* **18**, 825 (2022).
11. Marti-Sabaté, M. & Torrent, D. Dipolar localization of waves in twisted phononic crystal plates. *Phys. Rev. Appl.* **15**, L011001 (2021).
12. Tan, Z. et al. Terahertz spin-conjugate symmetry breaking for nonreciprocal chirality and one-way transmission based on magneto-optical moiré metasurface. *Adv. Sci.* **10**, 2204916 (2022).
13. Dong, K., Zhang, T., Li, J., & Yao, J. Flat bands in magic-angle bilayer photonic crystals at small twists. *Phys. Rev. Lett.* **126**, 223601 (2021).
14. Peotta, S. & Törmä, P. Superfluidity in topologically nontrivial flat bands. *Nat. Commun.* **6**, 8944 (2015).
15. Sun, T. et al. Van der Waals quaternary oxides for tunable low-loss anisotropic polaritonics. *Nat. Nanotechnol.* **19**, 758–765 (2024).
16. Duan, J., Nikitin, A. Y. & Alonso-González, P. Multiple and spectrally robust photonic magic angles in reconfigurable α-MoO_3 trilayers. *Nat. Mater.* **22**, 867–872 (2023).
17. Tarnopolsky, G., Kruchkov, A. J. & Vishwanath, A. Origin of magic angles in twisted bilayer graphene. *Phys. Rev. Lett.* **122**, 106405 (2019).
18. Wang, L., Shih, E., Runbio, A., Pasupathy, A. & Dean, C. Correlated electronic phases in twisted bilayer transition metal dichalcogenides. *Nat. Mater.* **19**, 861–866 (2020).
19. Morissette, E., Mounce, A. & Li, J. I. A. Dirac revivals drive a resonance response in twisted bilayer graphene. *Nat. Phys.* **19**, 1156 (2023).
20. Cao, Y. et al. Tunable correlated states and spin-polarized phases in twisted bilayer–bilayer graphene. *Nature* **583**, 215–220 (2020).
21. Sivadas, N., Okamoto, S., Xu, X., Fennie, C. J. & Xiao, D. Stacking dependent magnetism in bilayer CrI3. *Nano Lett.* **18**, 7658–7664 (2018).
22. Yves, S. et al. Moiré-driven topological transitions and extreme anisotropy in elastic metasurfaces. *Adv. Sci.* **9**, 2200181 (2022).
23. Han, C. L. et al. Nonlocal acoustic moiré hyperbolic metasurfaces. *Adv. Mater.* **14**, 2311350 (2024).
24. Liu, X. et al. Spectroscopy of a tunable moiré system with a correlated and topological flat band. *Nat. Commun.* **12**, 2732 (2021).
25. Khalaf, E., Kruchkov, A. J., Tarnopolsky, G. & Vishwanath, A. Magic angle hierarchy in twisted graphene multilayers. *Phys. Rev. B* **100**, 085109 (2019).
26. Andrei, E. Y. & MacDonald, A. H. Graphene bilayers with a twist. *Nat. Mater.* **19**, 1265–1275 (2020).
27. Burg, G. et al. Emergence of correlations in alternating twist quadrilayer graphene. *J. Nat. Mater.* **21**, 884 (2022).

28. Zhang, Q. et al. Interface nano-optics with van der Waals polaritons. *Nature* **597**, 187 (2021).
29. Lu, X. et al. Superconductors, orbital magnets and correlated states in magic-angle bilayer graphene. *Nature* **574**, 653 (2019).
30. Yi, C.-H., Park, H. C. & Park, M. J. Strong interlayer coupling and stable topological flat bands in twisted bilayer photonic moiré superlattices. *Light. Sci. Appl.* **11**, 289 (2022).
31. Tang, H., Du, F., Carr, S. & Mazur, E. Modeling the optical properties of twisted bilayer photonic crystals. *Light. Sci. Appl.* **10**, 157 (2021).
32. Tang, H., Ni, X., Du, F., Srikrishna, V. & Mazur, E. On-chip light trapping in bilayer moiré photonic crystal slabs. *Appl. Phys. Lett.* **121**, 231702 (2022).
33. Balents, L., Dean, C. R., Efetov, D. K. & Young, A. F. Superconductivity and strong correlations in moiré flat bands. *Nat. Phys.* **16**, 725–733 (2020).
34. Chen, M. et al. Configurable phonon polaritons in twisted α-MoO_3. *Nat. Mater.* **19**, 1307 (2020).
35. Gao, W. et al. Topological photonic phase in chiral hyperbolic metamaterials. *Phys. Rev. Lett.* **114**, 037402 (2014).
36. Hu, G. et al. Topological polaritons and photonic magic angles in twisted α-MoO_3 bilayers. *Nature* **582**, 209–213 (2020).
37. Hu, G., Krasnok, A., Mazor, Y., Qiu, C. & Alù, A. Moiré hyperbolic metasurfaces. *Nano Lett.* **20**, 3217–3224 (2020).
38. Yves, S., Peng, Y. & Alù, A. Topological Lifshitz transition in twisted hyperbolic acoustic metasurfaces. *Appl. Phys. Lett.* **121**, 122201 (2022).
39. Zheng, C. et al. Molding broadband dispersion in twisted trilayer hyperbolic polaritonic surfaces. *ACS Nano* **16**, 13241–13250 (2022).
40. Lee, K. et al. Discovery of a weak topological insulating state and van Hove singularity in triclinic $RhBi_2$. *Nat. Commun.* **12**, 1855 (2021).
41. Wang, S. et al. Highly crystalline rubrene light-emitting diodes with epitaxial growth. *Adv. Funct. Mater.* **33**, 2213768 (2023).
42. Ma, W. et al. Ghost hyperbolic surface polaritons in bulk anisotropic crystals. *Nature* **596**, 362–366 (2021).
43. Hu, G. et al. Real-space nanoimaging of hyperbolic shear polaritons in a monoclinic crystal. *Nat. Nanotechnol.* **18**, 64–70 (2023).
44. Kotov, O. & Lozovik, Y. Hyperbolic hybrid waves and optical topological transitions in few-layer anisotropic metasurfaces. *Phys. Rev. B.* **100**, 165424 (2019).
45. Kim, S. E., Erhart, P., Cahill, D. & Park, J. Extremely anisotropic van der Waals thermal conductors. *Nature* **597**, 660–665 (2021).
46. Dukhin, A. S. & Goetz, P. J. Bulk viscosity and compressibility measurements using acoustic spectroscopy. *J. Chem. Phys.* **130**, 124519 (2009).
47. Nguyen, D. X. et al. Magic configurations in moiré superlattice of bilayer photonic crystal: almost-perfect flatbands and unconventional localization. *Phys. Rev. Res.* **4**, L032031 (2022).
48. Ni, X. et al. Three-dimensional reconfigurable optical singularities in bilayer photonic crystals. *Phys. Rev. Lett.* **132**, 073804 (2024).
49. Zhuang, Z.-P., Zeng, H.-L., Chen, X.-D., He, X.-T. & Dong, J.-W. Topological nature of radiation asymmetry in bilayer metagratings. *Phys. Rev. Lett.* **132**, 113801 (2024).

Acknowledgements

T.-Z.Y. and C.-Y.L. acknowledge support from the National Natural Science Foundation of China [Grant No. 12232014], the Natural Science Foundation of China [Grant No. 12072221], the Fundamental Research Funds for the Central Universities [Grant No. 2013017] and the Ten Thousand Talents. C.-L.H. acknowledges the support of China Scholarship Council [Grant No. 202406080122] and the Fundamental Research Funds for the Central Universities [Grant No. N2403003]. L.-Q.C. acknowledges support from the Science Center Program of National Natural Science Foundation of China (Grant No. 62188101), and the National Natural Science Foundation of China (Grant No. 12132002). C.-W.Q. acknowledges financial support from the Ministry of Education, Singapore (Grant No. A-8000107-01-00).

Author contributions

C.-L.H., S.-D.F., and H.-T.Z. contribute equally to this work. C.-W.Q., T.-Z.Y., X.-D.Y., and L.-Q.C. conceived the idea. C.-L.H., S.-D.F., and H.-Z.L. performed the experiments. C.-L.H., S.-D.F., Y.-R.J., C.-Y.L., and K.H. carried out the theoretical analysis and simulations. C.-L.H., H.-T.Z., and T.-Z.Y. wrote the manuscript with contributions from the other authors. All of the authors have made a substantial contribution to the paper.

Competing interests

The authors declare no competing interests.

Additional information

Supplementary information The online version contains supplementary material available at https://doi.org/10.1038/s41467-025-55937-4.

Correspondence and requests for materials should be addressed to Xiao-Dong Yang, Tianzhi Yang or Cheng-Wei Qiu.

Peer review information *Nature Communications* thanks the anonymous reviewers for their contribution to the peer review of this work. A peer review file is available.